

## Analysis and Design of VCO-Based Phase-Domain $\Sigma\Delta$ Modulators

Sönmez, Uğur; Sebastiano, Fabio; Makinwa, Kofi A.A.

**DOI**

[10.1109/TCSI.2016.2638827](https://doi.org/10.1109/TCSI.2016.2638827)

**Publication date**

2017

**Document Version**

Accepted author manuscript

**Published in**

IEEE Transactions on Circuits and Systems Part 1: Regular Papers

**Citation (APA)**

Sönmez, U., Sebastiano, F., & Makinwa, K. A. A. (2017). Analysis and Design of VCO-Based Phase-Domain  $\Sigma\Delta$  Modulators. *IEEE Transactions on Circuits and Systems Part 1: Regular Papers*, 64(5), 1075-1084. [7817814]. <https://doi.org/10.1109/TCSI.2016.2638827>

**Important note**

To cite this publication, please use the final published version (if applicable). Please check the document version above.

**Copyright**

Other than for strictly personal use, it is not permitted to download, forward or distribute the text or part of it, without the consent of the author(s) and/or copyright holder(s), unless the work is under an open content license such as Creative Commons.

**Takedown policy**

Please contact us and provide details if you believe this document breaches copyrights. We will remove access to the work immediately and investigate your claim.

# Analysis and Design of VCO-Based Phase-Domain $\Sigma\Delta$ Modulators

Uğur Sönmez, *Member, IEEE*, Fabio Sebastiano, *Member, IEEE*, and Kofi A. A. Makinwa, *Fellow, IEEE*

**Abstract**— VCO-based phase-domain  $\Sigma\Delta$  modulators employ the combination of a voltage-controlled-oscillator (VCO) and an up/down counter to replace the analog loop filter used in conventional  $\Sigma\Delta$  modulators. Thanks to this highly digital architecture, they can be quite compact, and are expected to shrink even further with CMOS scaling. This paper describes the analysis and design of such converters. Trade-offs between design parameters and the impact of non-idealities, such as finite counter length and VCO non-linearity, are assessed through both theoretical analysis and behavioral simulations. The proposed design methodology is applied to the design of a phase-to-digital converter in a 40-nm CMOS process, which is used to digitize the output of a thermal-diffusivity temperature sensor, achieving  $\pm 0.2^\circ$  ( $3\sigma$ ) phase inaccuracy from  $-40$  to  $125^\circ\text{C}$  and a sensor-limited resolution of  $57\text{ m}^\circ$  (RMS) within a 500-Hz bandwidth. Measurements on the prototype agree quite well with theoretical predictions, thus demonstrating the validity of the proposed design methodology.

**Index Terms**— VCO-based Sigma-Delta modulator, Time-to-digital converter, Phase-to-digital converter, Quantization noise

## I. INTRODUCTION

IN recent years, time-to-digital converters (TDCs) have found many applications, especially in digital PLLs and instrumentation applications [1][2]. One specific class of TDCs, known as phase-to-digital converters, can be used to digitize the phase of a periodic input signal. Phase-to-digital converters based on the  $\Sigma\Delta$  ADC architecture, i.e. phase-domain  $\Sigma\Delta$  modulators (PDE $\Sigma\Delta$ s), have been used in readout circuits for single-photon avalanche diodes (SPADs) [3], wireless receivers [4], resistor-based temperature sensors [5], and thermal-diffusivity-based (TD) temperature sensors [6].

Fig. 1 shows a simplified block diagram of a PDE $\Sigma\Delta$ M. Here, an input signal ( $V_{IN}$ ) at frequency  $F_{IN}$  and with a phase shift  $\Phi_{IN}$  is multiplied by the clock signal  $V_{DEM}$ , which is at the same carrier frequency as  $V_{IN}$  ( $F_{DEM} = F_{IN}$ ). This results in a DC component proportional to their phase difference, as well as higher order components. The multiplier's output is applied to a loop filter, which in the case of a 1<sup>st</sup>-order modulator is an integrator [7]. The loop filter drives an  $M$  bit quantizer, which,

in turn, drives an  $M$  bit phase DAC that adjusts the phase of  $V_{DEM}$ . The loop attempts to minimize the DC component at the integrator input in a  $\Sigma\Delta$  manner, and as a result, the output bitstream is a digital representation of the signal phase  $\Phi_{IN}$ .

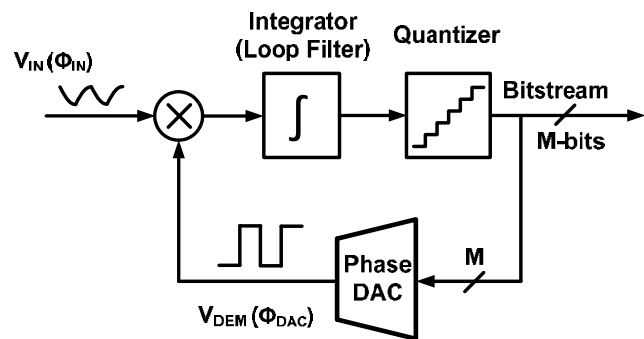


Fig. 1. Block diagram of an analog PDE $\Sigma\Delta$ M.

The architecture of a PDE $\Sigma\Delta$ M is similar to that of an analog PLL, and as such it is capable of rejecting wide-band noise while detecting the phase of an input signal relative to that of a reference. This property has been exploited for the readout of temperature sensors based on the thermal diffusivity (TD) of silicon [6]-[8]. Such TD sensors output a small (millivolt-level) signal, whose phase-shift is a function of temperature, but which is accompanied by relatively large amounts of wide-band noise. Since their accuracy improves with process scaling, smart TD sensors, i.e. TD sensors with a digital output, are well suited for the thermal management of SoCs. In such applications, however, area is at a premium, and so most published designs occupy less than  $10,000\ \mu\text{m}^2$  [10][11]. This in turn puts pressure on the area of the PDE $\Sigma\Delta$ M, which currently dominates the area of smart TD sensors.

This issue has been addressed by the adoption of a highly digital PDE $\Sigma\Delta$ M based on a voltage-controlled oscillator (VCO), first implemented in a mature  $0.16\text{-}\mu\text{m}$  CMOS process [8], and later shown to scale in a more advanced 40-nm CMOS process [9]. Inspired by compact VCO-based ADCs [12][13], a VCO translates the input signal into the frequency domain. The phase-shift of this frequency-domain signal is then digitized by an all-digital phase-domain ADC based on an up/down counter,

This paper was submitted for review on 21<sup>st</sup> of June, 2016. This work was supported in part by the Dutch Technology Foundation STW.

Uğur Sonmez is with Electronic Instrumentation Lab., part of Delft University of Technology in Mekelweg 4, 2628CD Delft, The Netherlands (e-mail: u.sonmez@tudelft.nl).

Fabio Sebastiano is with Delft University of Technology in Mekelweg 4, 2628CD Delft, The Netherlands (e-mail: f.sebastiano@tudelft.nl).

Kofi A. A. Makinwa is with Delft University of Technology in Mekelweg 4, 2628CD Delft, The Netherlands (e-mail: f.sebastiano@tudelft.nl).

which acts as an integrator. Thanks to this highly digital architecture, such VCO-based P $\Sigma\Delta$ Ms take full advantage of technology scaling, as proven by a x3 smaller area and x2 less supply voltage requirement when ported from 0.16- $\mu$ m to 40-nm CMOS [8][9]. However, an analysis of this architecture discussing potential drawbacks and design trade-offs, has not yet been reported.

This paper will analyze the unique features of VCO-based P $\Sigma\Delta$ Ms that differentiate them from VCO-based ADCs and analog-based P $\Sigma\Delta$ Ms. Section II will describe the operation of a general multi-bit VCO-based P $\Sigma\Delta$ M. The quantization error associated with its digital counter is discussed in section III. Section IV discusses the design of the digital counter, based on counter wrap-around constraints. The effect of non-linearity is tackled in section V. A second order modulator with potentially higher SNR is presented in section VI. In section VII, the developed models will be used to go through the design procedure of a prototype first-order P $\Sigma\Delta$ M and expected performance will be compared to experimental results. Finally, the conclusions highlights how the proposed design procedure can lead to area-efficient VCO-based P $\Sigma\Delta$ Ms with performance comparable to analog-based designs.

## II. VCO-BASED P $\Sigma\Delta$ M ARCHITECTURE

The VCO-based version of this architecture is shown in Fig. 2(a).  $V_{IN}$  is converted into variations of the VCO's output frequency. The counter acts like an integrator, while its up-down input ( $DEM$ ) facilitates chopper demodulation, i.e. multiplication by a square wave, since it determines whether the counter's state is either incremented or decremented. The value accumulated by the counter after one cycle of  $DEM$  will then be proportional to the integrated phase-shift between  $DEM$  and the VCO's output frequency, thus emulating the function of an integrator.

This highly digital implementation avoids the need for the large capacitors usually employed in analog loop filters and enables an efficient implementation of the  $M$  bit quantizer, which can be realized by sampling the  $M$  MSB's of the digital integrator output.

For maximum accuracy, both analog and VCO-based modulators are usually operated as incremental converters, in which the integrator is reset before each conversion [14]. A sinc filter (implemented by a simple counter) can then be used to decimate the converter's output [14]. An implementation of the first order VCO-based P $\Sigma\Delta$ M is shown in Fig. 2 (b). An  $S$  bit up/down counter is used to combine demodulation and integration, while an  $M$  bit register acts as the quantizer. The quantizer sampling clock ( $F_s$ ) is typically chosen at the same frequency as  $F_{DEM}$  [7].

In order to prevent meta-stability problems in the counter, a flip-flop is used to synchronize the up/down signal to the next edge of  $F_{VCO}$ . This is similar to the clock re-synchronization [15] required when two clock domains cross each other. This re-synchronization clock is shown as  $F_{SYNC}$  in Fig. 2(b).

## III. NOISE ANALYSIS AND COUNTER QUANTIZATION

The VCO-based P $\Sigma\Delta$ M has three major noise sources:  $\Sigma\Delta$  quantization noise, up/down counter's quantization error and

VCO's phase noise. As is well-known, the  $\Sigma\Delta$ 's quantization noise can be reduced by increasing  $M$ , its order or sampling rate [18].

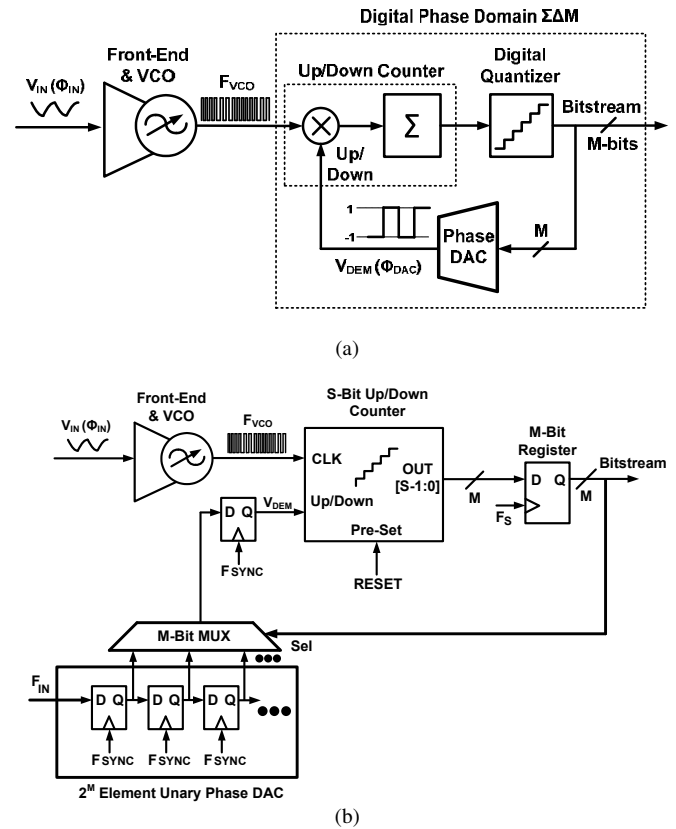


Fig. 2. (a) Block diagram, and (b) circuit-level implementation of the VCO-based P $\Sigma\Delta$ M architecture.

The second noise source, due to up/down counter's quantization, is unique to VCO and counter based  $\Sigma\Delta$  modulators. Unlike an analog integrator, an up/down counter can only count integer values and hence imposes rounding on its input. In the following, a simple expression for the quantization noise associated with the operation of the up/down counter will be derived.

For this analysis, we will model the counter as an ideal discrete-time integrator that introduces some input-referred quantization error at the end of every up/down cycle. The timing diagram in Fig. 3 shows how this simplification can be made. Here, we are also assuming that the input carrier signal is a sinusoid with frequency  $F_{IN}$  and a signal phase shift  $\Phi_{IN}$  with respect to the reference square-wave up/down signal with  $\Phi_{DAC} = 0$ .

The frequency of the VCO ( $F_{VCO}$ ) can be expressed as:

$$F_{VCO}(t) = K_{VCO}V_A \cos(2\pi F_{IN}t + \Phi_{IN}) + F_{NOM} \quad (1)$$

where  $K_{VCO}$  is the VCO gain,  $V_A$  is the amplitude of the input carrier and  $F_{NOM}$  is the nominal VCO output frequency. After integrating  $F_{VCO}$  for each full up period ( $\tau_{UP}$ ) and a full down period ( $\tau_{DOWN}$ ), an ideal counter, i.e. a counter without any quantization error, would compute the residual count  $C$  given by:

$$C = \int_0^{\tau_{UP}} F_{VCO}(t) dt - \int_{\tau_{UP}}^{\tau_{UP} + \tau_{DOWN}} F_{VCO}(t) dt \quad (3)$$

Every period,  $C$  is computed and then accumulated with the previous result. For an up/down signal with a duty cycle of 50% ( $\tau_{UP} = \tau_{DOWN} = 0.5/F_{IN}$ ),  $C$  becomes:

$$C = \frac{2K_{VCO}V_A}{\pi F_{IN}} \sin(\Phi_{IN}) \quad (4)$$

It should be noted that while an exact 50% duty cycle can be guaranteed by a fully digital chopper, the mismatch or duty-cycle errors of an analog chopper will result in residual offset [16]. The absence of residual chopper offset is a distinct advantage of this architecture.

Shifting the phase of the up/down signal by  $\Phi_{DAC}$  (due to the phase DAC action) is equivalent to shifting the input signal by  $-\Phi_{DAC}$ ; thus a more general form of (4) is:

$$C = \frac{2K_{VCO}V_A}{\pi F_{IN}} \sin(\Phi_{IN} - \Phi_{DAC}) \quad (5)$$

During regular  $\Sigma\Delta$  operation, the feedback loop ensures that on average  $\sin(\Phi_{IN} - \Phi_{DAC}) = 0$ . Since  $\sin(\Phi_{IN} - \Phi_{DAC}) \approx \Phi_{IN} - \Phi_{DAC}$  for small phase differences, we can model the relationship between  $C$  and phase as a gain factor  $K$  (Fig. 4). The phase-to-count gain  $K$  can be readily defined from (5) as:

$$K = \frac{2K_{VCO}V_A}{\pi F_{IN}} \quad (6)$$

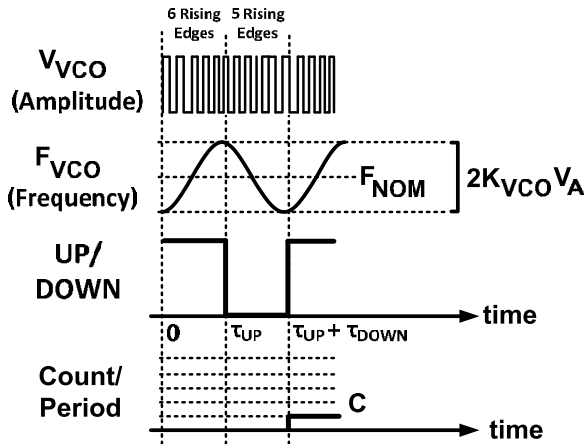


Fig. 3 Timing diagram demonstrating how up/down counting can be modeled as a combination of chopping and discrete-time integration.

However, a digital counter can only accumulate integer values because it only responds to the edges of  $F_{VCO}$ , which is equivalent to rounding  $C$  to an integer before the accumulation operation. Fig. 5 demonstrates the timing diagram resulting from such synchronization. With this additional synchronization step, the quantization is in essence a “round up” operation, where the counter is able to round up the fractional count at its input before integration. The errors  $\Delta Q_U(N)$  and  $\Delta Q_D(N)$  denote the fractional count error at the  $N^{\text{th}}$  cycle in the up and down period, respectively, and as round-up errors, they are bounded by [0 1] (Fig. 5).

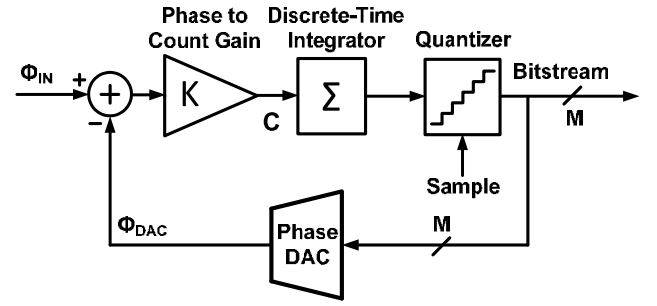


Fig. 4. Block diagram of the ideal discrete-time PDSΔM with a discrete-time integrator.

$\Delta Q_U(N)$  and  $\Delta Q_D(N)$  are deterministic for a given  $F_{VCO}$  and up/down signal. As will be shown later, VCO's accumulated jitter at the  $N^{\text{th}}$  cycle will randomize the timing and duration of events  $\Delta Q_U(N)$  and  $\Delta Q_D(N)$ . Thus, the VCO will introduce significant dithering, and the quantization error can be assumed to be uniformly and randomly distributed on the [0 1] interval and uncorrelated in time.

This is analogous to approximating as white noise the quantization error introduced by the comparator of a  $\Sigma\Delta$  modulator [17]. Noting that the average quantization error is 0.5, the variance of  $\Delta Q_U(N)$  and  $\Delta Q_D(N)$  can then be computed as [18]:

$$\sigma_q^2 = \int_0^1 (q - 0.5)^2 dq = \frac{1}{12} \quad (7)$$

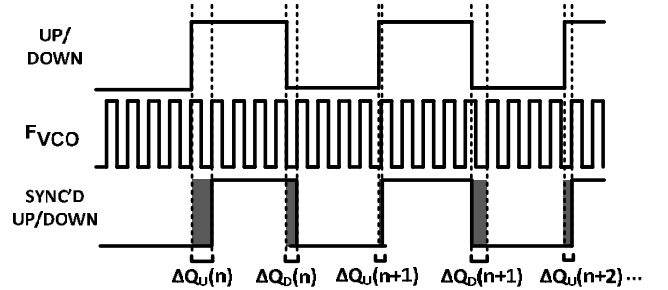


Fig. 5. Timing diagram demonstrating the error introduced by metastability synchronization of up/down signal to  $F_{VCO}$ .

As can be seen on Fig. 5, the total error for the  $N^{\text{th}}$  cycle  $[\Delta Q_T(N)]$  is given by the error on the up period minus the error on the down period

$$\begin{aligned} \Delta Q_T(N) &= [\Delta Q_U(N) - \Delta Q_D(N)] - [\Delta Q_D(N) - \Delta Q_U(N+1)] \\ &= \Delta Q_U(N) - 2\Delta Q_D(N) + \Delta Q_U(N+1) \end{aligned} \quad (8)$$

The total error after  $N$  up/down cycles can be written as the sum of the following series:

$$\begin{aligned} \sum_{k=1}^N \Delta Q_T(k) &= \Delta Q_U(1) - 2\Delta Q_D(1) + 2\Delta Q_U(2) - 2\Delta Q_D(2) \\ &\quad + \dots + \Delta Q_U(N+1) \end{aligned} \quad (9)$$

Since each element in the series has a variance of  $\sigma_q^2$ , and is assumed to be uncorrelated from the others, the variance of the total error is equal to the sum of all component variances:

$$\sigma^2 \left( \sum_{k=1}^N \Delta Q_T(k) \right) = (8N - 2) \sigma_Q^2 \quad (10)$$

while the mean of the total error is zero. When  $N \gg 1$ , this error converges to  $8N\sigma_Q^2$ . The bandwidth of this error is  $F_{IN}/2$ , since it manifests every time an up/down count period is completed. Using (7), we get the total power of the error in fractional counts ( $\sigma_{TOTAL}^2$ ) for a bandwidth  $F_{BW}$ :

$$\sigma_{TOTAL}^2 = \frac{4 F_{BW}}{3 F_{IN}} \quad (11)$$

If the sampling rate ( $F_S$ ) of the PD $\Sigma\Delta$ M is chosen equal to  $F_{IN}$ , then the ratio  $F_S/2F_{BW}$  is also known as the oversampling ratio ( $OSR$ ) of the  $\Sigma\Delta$  modulator.

Now, we can replace the discrete-time block in Fig. 4 with an integrator and an additive white noise source ( $\Delta Q_{ERR}$ ) with a power of  $\sigma_{TOTAL}^2$ , as shown in Fig. 6.

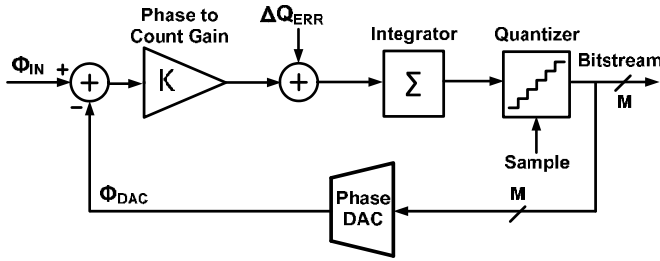


Fig. 6. Block diagram of the PD $\Sigma\Delta$ M with white additive noise source modelling the counter quantization noise.

The error in fractional counts can be directly converted into phase, which results in an input-referred phase error with an in-band power of  $\sigma_p^2$ , where:

$$\sigma_p^2 = \frac{2}{3 \cdot OSR \cdot K^2} \quad (12)$$

By using (6), the RMS in-band error in radians ( $\sigma_{p,r}$ ) is:

$$\sigma_{p,r}(\text{in-band}) = \sqrt{\frac{1}{6OSR} \cdot \frac{\pi F_{IN}}{K_{VCO} V_A}} \quad (13)$$

Looking at (13), we can make an important conclusion: the input-referred quantization noise due to the digital counter scales inversely with the product of signal amplitude and VCO gain, i.e. the frequency swing at the VCO output. For a given  $F_{IN}$  and  $V_A$ ,  $K_{VCO}$  or  $OSR$  must be increased to suppress such quantization noise. Since a larger  $OSR$  implies a lower conversion speed, increasing  $K_{VCO}$  is more desirable.

This analysis has been also confirmed by system-level simulations, i.e. the simulation of an ideal  $\Sigma\Delta$  modulator with additive noise (to breakup strong idle tones) as shown in Fig. 6 (simulated in Matlab), and a mixed-signal simulation in CppSim [19].

In both models,  $K_{VCO}V_A = 70$  MHz,  $F_{IN} = F_S = 1.17$  MHz,  $F_{NOM} = 600$  MHz,  $S = 8$  and  $M = 3$ . The phase DAC spans

78.75° with steps of 11.25°. A block diagram of the mixed-signal CppSim model is shown in Fig. 7. A high-frequency clock ( $F_{SYNC}$ ) is used to generate the 3-bit phase DAC values ranging from 11.25° to 90°. The up/down counter was compiled as a Verilog block, and is hence ideal. Standard D flip-flop, VCO and multiplexer elements were used from CppSim's standard libraries.

Fig. 8 shows the power spectral density (PSD) simulated in the two models together with the quantization noise floor calculated from (13) (dashed blue line). Good agreement is achieved at low frequencies between both models and the theoretical prediction. The quantization noise is predicted to be 38 m° for  $OSR = 1024$ , which corresponds to ~1 ms conversion time. The idle tone around 400 kHz for the CppSim model results is attributed to the limited accuracy of the time-domain model (100 ps). The idle tone is not observed in measurement results. Although low-frequency idle tones are a typical issue for 1<sup>st</sup>-order modulator, they do not appear in the simulation shown in Fig. 8 because of the dithering action of the thermal noise superimposed on the input signal. In typical sensing applications of the phase-domain read-out, such as those shown in section VII, the input signal is characterized by a small amplitude and relatively large noise that is enough to dither the modulator.

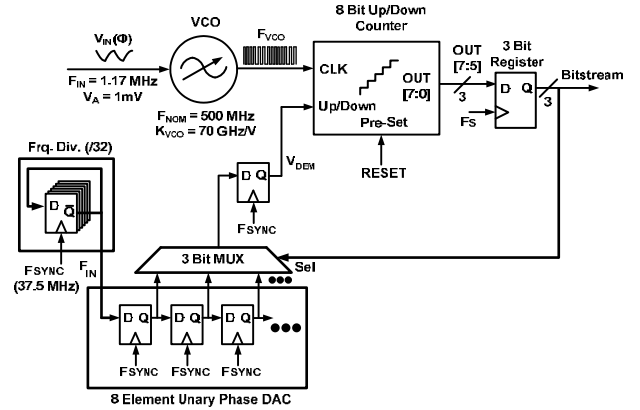


Fig. 7. Block diagram of the implemented CppSim model.

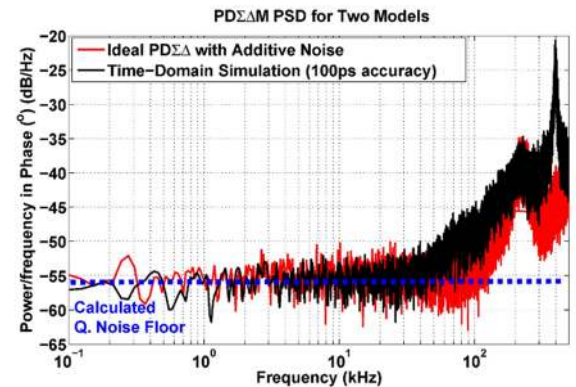


Fig. 8. Power spectral density of the output bitstream of an ideal  $\Sigma\Delta$  model with additive noise and of a transient simulation.

The agreement of the two models with (13) means that long time-domain simulations can be avoided when only the in-band behavior of the counter's quantization noise is of interest, since

a simple noise source at the input of the discrete-time integrator is sufficient to capture its low-frequency noise behavior.

Once the counter quantization noise is calculated, we can determine the VCO's phase noise requirement. For this analysis we assume that thermal noise dominates the VCO phase noise. In order to make the analysis consistent with the model in Fig. (6), we first derive the effect of phase noise in terms of fractional counts and then refer the error back to phase.

First, we assume a fractional frequency power spectral density (PSD)  $S_Y(f)$  due to phase noise. For simplicity, we also assume  $F_{VCO} = F_{NOM}$ .

From (3), we can convert  $S_Y(f)$  into fractional count PSD  $S_C(f)$ . Up/down modulation acts as a chopper, or a mixer, and down-modulates to DC the frequency noise spectrum around  $F_{IN}$ , where  $F_{IN}$  is the modulation frequency [16]. Without up/down operation, counter output is simply  $F_{NOM}$  times the count period of  $2\tau_{UP}$ , so:

$$S_C(f) = 4\tau_{UP}^2 F_{NOM}^2 S_Y(f + F_{IN}) \quad (14)$$

We can relate  $S_Y(f)$  to VCO's phase noise  $\mathcal{L}_\Phi(f)$  [26]:

$$S_Y(f) = 2\mathcal{L}_\Phi(f) \frac{f^2}{F_{NOM}^2} \quad (15)$$

By combining (14) with (5) and (15), we get the PSD of the input-referred noise as:

$$S_{\Phi IN}(f) = \frac{\pi^2}{2K_{VCO}^2 V_A^2} \mathcal{L}_\Phi(f + F_{IN})(f + F_{IN})^2 \quad (16)$$

Note that  $S_{\Phi IN}(f)$  is the equivalent noise on the input phase signal and it is different from the VCO phase noise  $\mathcal{L}_\Phi(f)$ . The variance due to  $S_{\Phi IN}(f)$  can be obtained by integrating  $S_{\Phi IN}(f)$  over the bandwidth of interest from DC up to  $F_{BW}$ . As expected, only the VCO phase noise at an offset  $F_{IN}$  from the carrier contributes to the output. Noise at lower frequencies (such as flicker noise) is suppressed because it will be up-modulated around  $F_{IN}$  by the up/down modulation and filtered by the decimation filter, which is analogous to the flicker-noise suppression in chopper amplifiers [16]. However, most practical VCOs can still exhibit flicker noise at an offset frequency from the carrier around and above  $F_{IN}$ . In that case, the flicker noise corner can be reduced by a wide-band low-noise amplifier that precedes the VCO [8]. If the system allows it, the carrier frequency  $F_{IN}$  can also be increased to avoid flicker noise, at the cost of additional quantization noise.

For  $K_{VCO}=140$  MHz/V and  $V_A = 0.5$  mV, the phase-noise-induced output noise will be below the quantization-noise-induced output noise if the VCO phase noise is below -65 dBc/Hz for offset frequencies above 1.17 MHz, which is easily attainable by low-power VCO's [20].

#### IV. COUNTER SIZE AND WRAP-AROUND

Due to practical limitations, the maximum counter output in a VCO-based PDS $\Delta$ M is limited, especially in compact readouts where the area of the counter must be minimized [9]. A possible issue is counter wrap-around, i.e. when the counter

overflows. In order to design the size of the counter, we will first investigate wrap-around.

A straightforward solution would be to design the counter with overflow protection. Here, we will first observe what happens when both the input and the DAC phase are fixed, i.e. without any  $\Sigma\Delta$  feedback. From (2) and (3), assuming equal up and down periods, the minimum size of a non-wrapping counter ( $C_{SIZE,non-wrap}$ ) is:

$$C_{SIZE,non-wrap} > \int_0^{\tau_{UP}} F_{VCO}(t) dt \quad (17)$$

Note that  $C_{SIZE,non-wrap}$  in this case must be at least larger than  $F_{NOM}\tau_{UP}$ , which is large (~8 bits) for typical values ( $F_{NOM} > 500$  MHz,  $\tau_{UP} > 100$  ns). A similar constraint also exists for the down-counting phase.

If the counter is allowed to wrap-around (or overload) between up/down counts, this limitation is relaxed because only the remainder after a sequence of up and down counts must be smaller than the counter size. This can be simply expressed as:

$$C_{SIZE,wrap} > C \quad (18)$$

where  $C$  is defined in (5), and does not depend on  $F_{NOM}$ . Wrap-around in this case simply means allowing the counter output to overflow, as shown in Fig. 9. Intuitively, (20) means that the  $\Sigma\Delta$  still operates correctly if the counter wraps around, as long as the output sampled by the quantizer is correct. This can be observed from Fig. 9, which shows how wrapping does not affect the latched counter result. Since a wrapping counter can be of smaller length and does not need any additional logic for overload detection, it is simpler and hence occupies less silicon area. Thus, we will assume the use of a wrapping counter in the following.

The problem in a wrapping counter occurs when the counter value wraps around at, or just before a sampling moment, as illustrated in Fig. 10. Since the error ruins the integrated history of the signal, it is not shaped by the  $\Sigma\Delta$  loop and introduces a significant error. The erroneous bits generated during the recovery process will corrupt the output and influence both the decimated output (i.e. the accuracy) and the resolution. The wrap-around can be avoided by limiting the counter's output swing, which is analogous to limiting the output swing of integrators in a regular  $\Sigma\Delta$  modulator to avoid amplifier saturation [21].

For a single-bit PDS $\Delta$ M, wrap-around can be avoided if the peak-to-peak swing of the latched counter value is less than half the counter length. In that case, the  $\Sigma\Delta$  output bit-stream is the sampled counter MSB, and we have:

$$C_{SIZE,wrap} = 2^S > 2(C_{MAX} - C_{MIN}) = 2C_{PP}; \quad (19)$$

$$S > \log_2(2C_{PP})$$

Where  $C_{PP}$  is the peak-to-peak swing of the counter and  $S$  is the number of bits of the counter. Since  $C_{PP}$  is dependent on the input signal amplitude ( $V_{IN}$ ) and VCO gain ( $K_{VCO}$ ), an interesting trade-off exists between counter size and quantization noise. For low quantization noise,  $V_{IN}$  and  $K_{VCO}$  need to be high [from (13)], which means a larger counter is necessary to avoid wrap-around.

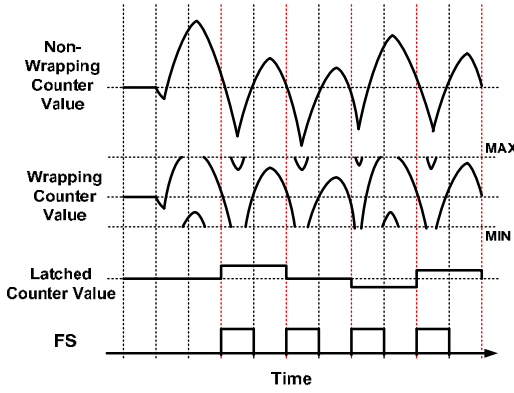


Fig. 9. Timing diagram showing how a wrapping counter can tolerate a smaller swing and counter size.

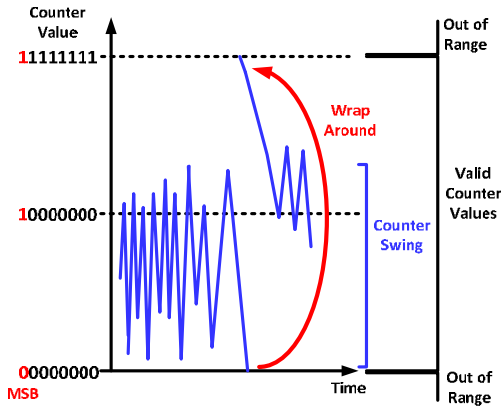


Fig. 10. Latched counter values of a single-bit PDSΔM with an 8-bit counter over time. If the counter wraps around, the output is corrupted for several successive samples.

$C_{PP}$  is bounded for a first-order modulator and is approximately constant over a bounded range of DC inputs [18]. A similar analysis can be made for an  $M$ -bit PDSΔM, as shown in Fig. 11. Counter wrap-around can be prevented if the peak-to-peak swing of the counter is guaranteed to be less than  $2^{S-M}$ . Therefore, for a general multi-bit case, we have:

$$C_{SIZE,wrap} = 2^{S-M} > C_{PP}, \text{ when } M > 1; \quad (20)$$

$$S > \log_2(C_{PP}) + M$$

As a convenient reliability measure, the input phase range can be restricted to be between the second highest and second lowest phase DAC steps, which relaxes (22) to  $S > \log_2(C_{PP}) + M - 1$ . An example of a PDSΔM used in a temperature sensor will demonstrate a typical  $C_{PP}$  value in section VII.

Another case where the counter can wrap-around is at the start of the conversion. This first count value can be very large and can cause a wrap-around. We will assume that the counter is reset to its median value ( $2^{S-1}$ ) and that the input phase is bounded within  $[0 \Delta]$ , where 0 and  $\Delta$  are the minimum and maximum value of the phase DAC ( $\Phi_{DAC}$ ), respectively. In this case, maximum value of  $|\Phi_{IN} - \Phi_{DAC}| \leq \Delta/2$ , and from (5), we find the maximum count ( $C_{MAX}$ ) to be:

$$C_{MAX} = \pm \frac{2K_{VCO}V_A}{\pi F_{IN}} \sin(\Delta/2) \quad (21)$$

To avoid wrap around, the following condition must hold:

$$S > \log_2 \left( \frac{2K_{VCO}V_A}{\pi F_{IN}} \sin(\Delta/2) \right) + 1 \quad (22)$$

Note that (21) and (22) hold for a multi-bit PDSΔM where  $|\Phi_{IN} - \Phi_{DAC}| \leq \Delta/2$ . For a single-bit modulator,  $\Phi_{IN} - \Phi_{DAC}$  can assume values up to  $\pm\Delta$ , and hence (21) and (22) must be modified by changing  $\Delta/2$  with  $\Delta$ .

The constraint imposed by (22) is different from (19) or (20), since it is not dependent on signal statistics. It is instead dependent on  $\Delta$ , i.e. the span of the phase DAC. Resetting the counter to  $2^{S-1}$  instead of another arbitrary value also helps minimizing the counter size.

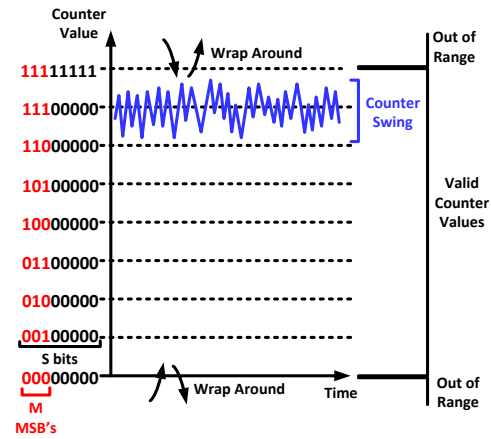


Fig. 11. Counter output of a 3-bit PDSΔM with an 8-bit counter over time.

## V. NON-LINEARITY

Because of the sine term in (5), the PDSΔM exhibits a systematic non-linearity. This non-linearity can either be corrected during digital post-processing [6], or by using small range(s) for  $\Phi_{DAC}$  [22], thus linearizing the sine term.

The non-linear relation between the average of the output bitstream ( $\mu$ ) and the input and DAC phase is described by the following equation for a single-bit PDSΔM:

$$\mu = \frac{\sin(\Phi_{IN} - \Phi_{DAC,1})}{\sin(\Phi_{IN} - \Phi_{DAC,1}) - \sin(\Phi_{IN} - \Phi_{DAC,0})} \quad (23)$$

where  $\Phi_{DAC,1}$  and  $\Phi_{DAC,0}$  are the DAC phases for a feedback values of 0 and 1. For multi-bit operation,  $\Phi_{DAC,1}$  and  $\Phi_{DAC,0}$  can be replaced with the exercised phase levels of the DAC. Note that although  $\mu$  itself is a non-linear function of  $\Phi_{IN}$ , it is independent of any circuit parameters, i.e. its non-linearity is systematic. However, additional non-linearities can shift this systematic curve, and add inaccuracy to the design.

From literature, VCOs are known to be highly non-linear with respect to the amplitude of their frequency-controlling input signal. For this reason, many techniques to improve VCO non-linearity have been adopted in VCO-based ADCs [23-25]. However, since the information in a PDSΔM is encoded in the

phase of the input signal, VCO non-linearity will have a smaller effect in the proposed read-out, as demonstrated in the following.

For a sinusoidal input as in (1), the VCO's amplitude non-linearity will produce tones at harmonics of  $F_{IN}$ . Considering only second and third harmonic of  $F_{IN}$ , the VCO output frequency can be expressed as:

$$F_{VCO}(t) = A_1 \cos(2\pi F_{IN}t + \Phi_{IN}) + A_2 \cos(4\pi F_{IN}t + 2\Phi_{IN}) + A_3 \cos(6\pi F_{IN}t + 3\Phi_{IN}) + F_{NOM} \quad (24)$$

where  $A_N$  is the amplitude of the  $N$ -th harmonic component. Combining (5) and (24), we get the total count after up/down periods as:

$$C = -\frac{2}{\pi F_{IN}} \left[ A_1 \sin(\Phi_{IN} - \Phi_{DAC}) + \frac{A_3}{3} \sin(3\Phi_{IN} - 3\Phi_{DAC}) \right] \quad (25)$$

Due to the up/down operation, the second harmonic cancels out and third harmonic only adds a gain error as long as  $3\Phi_{IN} - 3\Phi_{DAC}$  is small, since  $\sin(3\Phi_{IN} - 3\Phi_{DAC})/3 \approx \Phi_{IN} - \Phi_{DAC}$ . This means that the linearity can be improved if  $\Phi_{IN} - \Phi_{DAC}$  is made smaller, as will be demonstrated by simulation in the following. However, in the general case, (27) is modified to:

$$\mu = \frac{A_1 \sin(\Delta\Phi_1) + \frac{A_3}{3} \sin(3\Delta\Phi_1)}{A_1 (\sin(\Delta\Phi_1) - \sin(\Delta\Phi_0)) + \frac{A_3}{3} (\sin(3\Delta\Phi_1) - \sin(3\Delta\Phi_0))} \quad (26)$$

where  $\Delta\Phi_1$  is  $\Phi_{IN} - \Phi_{DAC,1}$  and  $\Delta\Phi_0$  is  $\Phi_{IN} - \Phi_{DAC,0}$ . In this case, the systematic non-linearity is a function of the ratio  $A_3/A_1$ , which strongly depends on the VCO circuit parameters. If  $A_3/A_1$  is fixed, the error can be eliminated by batch trimming but any spread will add inaccuracy.

From (26), we can make an important conclusion: First order errors in absolute values of  $A_1$  or  $A_3$  do not influence  $\mu$ . This is important in sensor applications, where changes in  $A_1$  (via  $K_{VCO}$ ) over temperature and other environmental effects are rejected by the system.

Any non-linearity in the VCO adds harmonic components of the input signal but does not cause any non-linear distortion in the phase of the fundamental tone. Since an ideal phase read-out is sensitive only to the phase of the fundamental, it is not affected by the VCO's amplitude distortion. Therefore, as the PDS $\Delta$ M behaves more closely to an ideal phase detector, for example using a smaller DAC phase range, it rejects VCO non-linearity better. As an example, we analyze the case where  $A_1/A_3 = 40$  dB for a single-bit modulator spanning a  $90^\circ$ -range ( $\Phi_{DAC,0} = 0^\circ, \Phi_{DAC,1} = 90^\circ$ ).  $A_1/A_3 = 40$  dB was chosen as a realistic third-order non-linearity of a typical VCO [12]. The non-linear error of such a PDS $\Delta$ M over the full range is shown in Fig. 14 (a) as the red curve. The blue curve shows the case where  $A_3 = 0$ , and the black curve shows the difference between the two cases. The VCO non-linearity causes a  $\pm 0.5^\circ$  error.

When the phase range, i.e. the maximum  $\Phi_{IN} - \Phi_{DAC}$ , is changed to  $11.25^\circ$ , as shown in Fig. 14 (b), the error then reduces to less than  $2$  m $^\circ$ . A reduction in the phase range can be easily achieved in multi-bit PDS $\Delta$ Ms or two-step PDS $\Delta$ Ms [7], thus making such architectures robust to the non-linearity of

typical VCO's, which show third-harmonic distortion ranging from  $-40$  to  $-60$  dB. It must be again highlighted that the high tolerance to distortion of the proposed read-out is an inherent property of phase-domain read-outs. Even a large distortion in the amplitude domain at the system input does not significantly affect the phase of the signal, which is the parameter carrying the information to be detected and converted.

However, the VCO's phase distortion or its signal-dependent delay will impact non-linearity. This necessitates the use of fast response VCO's or constant-bandwidth gain stages to drive the VCO, in order to control its delay. As an example, for a temperature sensor application [8], the gm-stage that drives the VCO needs to be biased with a PTAT current to improve linearity.

Current-starved inverters or simply current-controlled oscillators (CCO) are a good candidate for implementation of VCOs in PDS $\Delta$ Ms [8] because a CCO can respond very quickly to changes in its biasing current. If this CCO is driven by a gm-stage [8], that gm-stage dominates the VCO's delay. A gm-stage can be designed to have a relatively signal-independent bandwidth and thus the VCO's delay is only a weak function of the input signal.

## VI. SECOND-ORDER MODULATOR

It is well known that first order  $\Sigma\Delta$  modulators are affected by idle tones if the input signal does not have enough white noise content [18][21]. In sensor applications working with small signals, the 1<sup>st</sup>-order system in Fig. 2(a) is sufficiently dithered for achieving proper quantization noise behavior. For higher resolution systems, input noise may not provide sufficient dithering and higher-order PDS $\Delta$ M may be required.

Fig. 15 shows the block diagram of a second-order fully-digital PDS $\Delta$ M, where the quantizer in Fig. 2 (a) has been replaced by a digital  $\Sigma\Delta$  modulator. A linear-feedback shift register (LFSR) can be used to add dither to the quantizer.

Secondary feedback is applied via the digital gain term  $G$ . The digital  $\Sigma\Delta$  itself can be operated at the relatively low sampling rate of the quantizer ( $F_s$ ). This results in a minimal power penalty when increasing the modulation order.

The system in Fig. 15 has been simulated in CppSim environment to observe the system's performance for a large input carrier amplitude  $V_A$ . Thus, the following values were chosen:  $V_A = 200$  mV,  $K_{VCO} = 5$  MHz/mV,  $F_{IN} = F_s = 1.17$  MHz,  $F_{NOM} = 1.5$  GHz,  $S = 12$ ,  $G = 512$  and  $M = 3$ . The phase DAC spans  $78.75^\circ$  with steps of  $11.25^\circ$ . The second counter was sized as 16-bits, and is clocked at a rate of  $F_s$ .

Fig. 16 shows the simulated power spectral density (PSD) of the second-order PDS $\Delta$ M with the chosen variables. When compared to the first-order modulator in Fig. 8, this modulator is able to accommodate a much larger input voltage swing and thus has 23 dB better SNR due to 14x increase in  $K_{VCO}V_A$ . This improvement in SNR comes at a cost of larger area, higher VCO frequency, and requirement for higher  $V_A$  and better VCO phase noise and linearity specs. In modern digital processes, the impact of additional area and higher VCO frequency can be negligible for applications requiring high-resolution from the PDS $\Delta$ M.



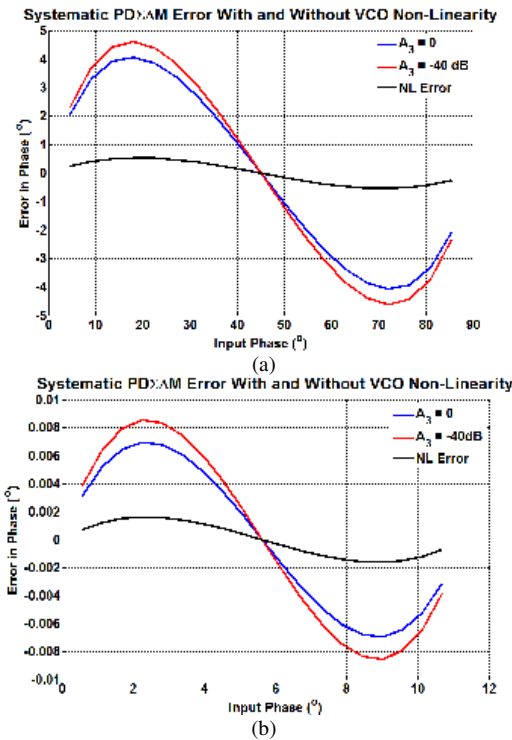


Fig. 14. Non-linearity error of a PDSΔM with and without the third order non-linearity from the VCO; with a phase DAC range of (a) 90° and (b) 11.25°

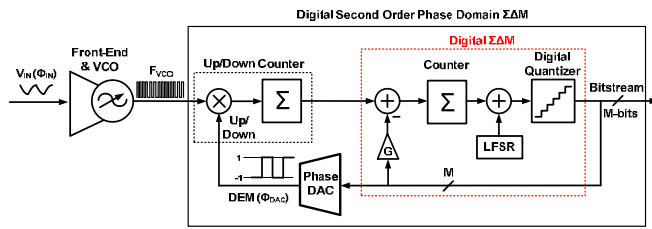


Fig. 15. Block diagram of a second-order VCO-based PDSΔM

As the amplitude of the input signal increases, VCO linearity becomes a critical practical problem. Larger input amplitude implies that both quantization and VCO phase noise contributes less, but the VCO will exhibit more distortion. This can be tackled using the techniques discussed in Section V.

## VII. AN EXAMPLE DESIGN: PDSΔM FOR TD TEMPERATURE SENSOR

In order to confirm the theoretical analysis presented in this work, we will consider the design and analysis of the multi-bit PDSΔM used to read out a thermal-diffusivity-based temperature sensor in a 40-nm CMOS process [9]. Specifications of the PDSΔM can be directly derived from the specifications of the temperature sensor. The input signal from the sensor is a filtered square-wave at  $F_{IN}=1.17$  MHz with roughly 1.3 mVpp amplitude, and a phase resolution of 47 m° (~0.8 mrad in radians) in a bandwidth of 500 Hz. This resolution includes the thermal noise generated by the sensor and also by the front-end amplifier. By choosing  $F_S = F_{IN} = 1.17$  MHz, an  $OSR > 1024$  is obtained for a 500-Hz bandwidth. The output phase from the sensor ranges from 11.25° to 90°, thus  $\Delta = 78.75^\circ$ .

In order not to degrade the sensor's resolution, we need to derive the  $K_{VCO}$  value that sufficiently suppresses the counter's quantization noise. We choose  $\sigma_{P,r} = 23$  m° [0.4 mrad in (13)], i.e. equal to half of the signal noise, which results in a 12% SNR degradation. From (13),  $K_{VCO}$  is then found to be 180 MHz/mV. In practice, since  $K_{VCO}$  can change dramatically due to process spread and temperature, we chose  $K_{VCO} = 200$  MHz/mV in the nominal case with worst-case of  $K_{VCO} = 160$  MHz/mV. Since we want to observe the worst cases for both resolution and wrap-around, we assume  $K_{VCO} = 160$  MHz/mV for quantization-noise calculation and 200 MHz/mV for wrap-around estimation.

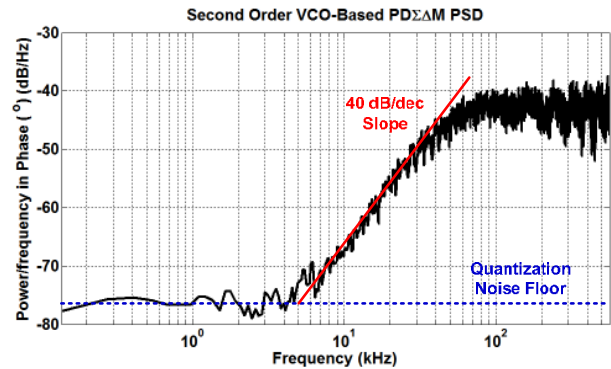


Fig. 16. Simulated PSD of the 2<sup>nd</sup> Order PDSΔM's output bitstream, generated via a transient simulation.

Experimental results also confirm this analysis. Fig. 17 shows the power spectral density (PSD) of the prototype sensor [9] as well as calculated counter quantization, thermal and combined noise densities. The sensors exhibit an RMS resolution of 1 mrad (0.36 °C for the temperature reading) within 500 Hz, which agrees well with a total computed RMS resolution of 0.95 mrad [0.8 mrad due to sensor noise; 0.45 mrad due to counter quantization noise according to (13)].

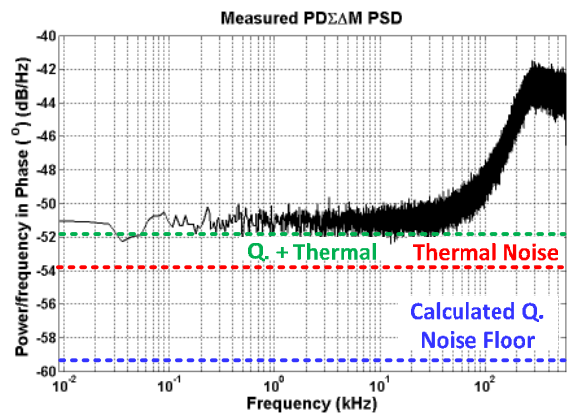


Fig. 17. Measured PSD of the prototype PDSΔM (8 million samples, averaged 8192 times); with expected noise densities.

The next step is determining the counter size ( $S$ ) from (20) and (22). The modulator is designed to span  $\Delta = 78.75^\circ$ , with a phase DAC range from 11.25° to 90°, resulting in  $S > 6.12$  from (24). For (20), we need to fix  $M$ , or the number of  $\Sigma\Delta$  modulator bits.  $M = 3$  was chosen as a good trade-off between phase DAC area and quantization noise suppression. The mixed-signal model in Fig. 7 for  $K_{VCO} = 200$  MHz/mV and  $\Phi_{IN} = 47^\circ$  was used to obtain a histogram of the counter output swing in Fig.

18 (a). In this model, thermal noise floor shown in Fig. 17 was added to the input. The peak-to-peak swing is 18 count values for 8192 samples. According to (20),  $2^{S-M} > 18$  to avoid wrap-around, which implies  $S \geq 8$ . This satisfies the requirement from (22) as well.

The simulated counter swing was compared to the measurement results in order to validate the simulation model. For this, the measured 3-bit MSBs of the counter (bit-stream) was compared to the 3-bit representation of the counter swing, shown on a histogram plot in Fig. 18 (b). For the measurement, 8192 samples were obtained also at  $\Phi_{IN} = 47^\circ$ . The measured and simulated histograms align, and the small difference between them is within the thermal noise budget.

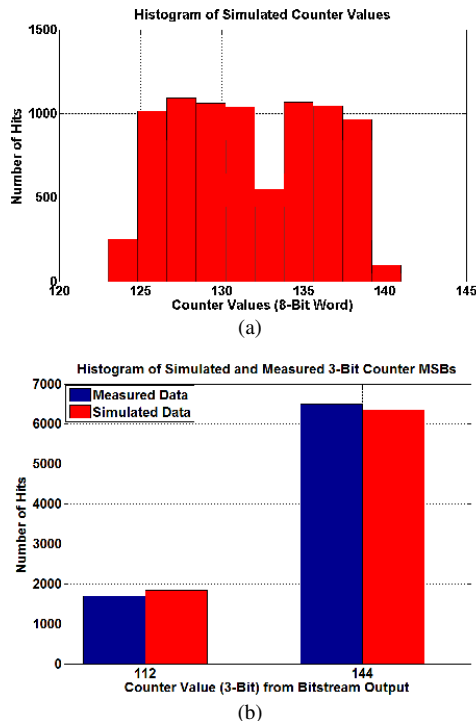


Fig. 18. (a) Histogram of simulated counter values for 8192 samples, showing the counter swing (b) Comparative 3-bit histogram of measured and simulated counter values

### VIII. CONCLUSIONS

This paper presents the first theoretical analysis of the operation of a VCO-based PDE $\Delta$ M. The derived theoretical model is shown to be in good agreement with both simulation and experimental results.

Quantization noise, counter wrap-around and settling time can add additional errors and design constraints in VCO-based PDE $\Delta$ Ms with respect to fully analog PDE $\Delta$ Ms. However, with enough VCO gain and a sufficient number of counter bits, the performance gap between analog and VCO-based modulators can be abridged. In addition, it has also been shown that the high non-linearity of practical VCO's can be tolerated by PDE $\Delta$ Ms. This allows the implementation of compact, scalable, mostly digital and accurate PDE $\Delta$ Ms, thus making them ideal for implementation in nanometer CMOS technologies.

### REFERENCES

- [1] J. P. Jansson, A. Mantyniemi and J. Kostamovaara, "A CMOS time-to-digital converter with better than 10 ps single-shot precision," *IEEE J. of Solid-State Circuits*, vol. 41, no. 6, pp. 1286-1296, June 2006.
- [2] R. B. Staszewski et al., "All-digital PLL and transmitter for mobile phones," *IEEE J. of Solid-State Circuits*, vol. 40, no. 12, pp. 2469-2482, Dec. 2005.
- [3] R.J. Walker, J.A. Richardson and R.K. Henderson, "A 128 $\times$ 96 pixel event-driven phase-domain  $\Delta\Sigma$ -based fully digital 3D camera in 0.13 $\mu$ m CMOS imaging technology," *Dig. Tech. ISSCC*, pp. 410-412, Feb. 2011.
- [4] Y. H. Liu et. Al., "A 1.2 nJ/bit 2.4 GHz Receiver With a Sliding-IF Phase-to-Digital Converter for Wireless Personal/Body Area Networks," *IEEE J. Solid-State Circuits*, vol.49, no 12., pp.3005-3017, Dec. 2014.
- [5] P. Park, D. Ruffieux and K.A.A. Makinwa, "A Thermistor-Based Temperature Sensor for a Real-Time Clock With  $\pm 2$  ppm Frequency Stability," *IEEE J. Solid-State Circuits*, vol.50, no 7., pp.1571-1580, July 2015.
- [6] C.P.L. van Vroonhoven and K.A.A. Makinwa, "A CMOS Temperature-to-Digital Converter with an Inaccuracy of  $\pm 0.5^\circ$  C ( $3\sigma$ ) from  $-55$  to  $125^\circ$ C," *Dig. Tech. ISSCC*, pp. 567-577, Feb. 2008.
- [7] U. Sonmez et. al., "A 0.008-mm<sup>2</sup> area-optimized thermal-diffusivity-based temperature sensor in 160-nm CMOS for SoC thermal monitoring," *ESSCIRC*, pp. 395-398, Sept. 2014
- [8] R. Quan et al., "A 4600 $\mu$ m<sup>2</sup> 1.5 $^\circ$ C ( $3\sigma$ ) 0.9kS/s Thermal-Diffusivity Temperature Sensor with VCO-Based Readout," *Dig. Tech. ISSCC*, pp.488-489, 2015.
- [9] U. Sonmez et al., "1650 $\mu$ m<sup>2</sup> Thermal-Diffusivity Sensors with Inaccuracies Down to  $\pm 0.75^\circ$ C in 40nm CMOS," *Dig. Tech. ISSCC*, pp.206-207, Feb. 2016.
- [10] T. Oshita et al., "Compact BJT-Based Thermal Sensor for Processor Applications in a 14 nm tri-Gate CMOS Process," *IEEE J. Solid-State Circuits*, vol. 50, no. 3, pp. 799-807, Feb. 2015.
- [11] J. Shor, and K. Luria, "Miniaturized BJT-based thermal sensor for microprocessors in 32- and 22-nm Technologies," *IEEE J. Solid-State Circuits*, vol. 48, no. 11, pp.2860-2867, Nov. 2013.
- [12] G. Taylor and I. Galton, "A Mostly-Digital Variable-Rate Continuous-Time Delta-Sigma Modulator ADC," *IEEE J. of Solid State Circuits*, vol. 45, no. 12, pp. 2634-2646, Sept. 2010.
- [13] M.Z. Straayer and M. Perrott, "A 12-Bit, 10-MHz Bandwidth, Continuous-Time  $\Sigma\Delta$  ADC With a 5-Bit, 950-MS/s VCO-Based Quantizer," *IEEE J. of Solid State Circuits*, vol. 43, no. 4, pp. 805-814, April 2008.
- [14] J. Robert et. al., "A 16-bit low-voltage CMOS A/D converter," *IEEE J. Solid-State Circuits*, vol. 22, no.2, pp. 157-163, April 1987.
- [15] R. B. Staszewski et. al., "All-digital phase-domain TX frequency synthesizer for Bluetooth radios in 0.13 $\mu$ m CMOS," *Dig. Tech. ISSCC*, pp. 272-273, Feb. 2004.
- [16] C. Enz, E. A. Vittoz, and F. Krummenacher, "A CMOS Chopper Amplifier," *IEEE J. of Solid State Circuits*, vol. 43, no. 22, pp. 335-342, June 1987.

- [17] R.M. Gray, "Oversampled Sigma-Delta Modulation," *IEEE Tran. On Communications*, vol. 35, no. 5, pp. 481-489, May 1987.
- [18] S.R. Norsworthy, R. Schreier and G. C. Temes, *Delta-Sigma Data Converters*, New York: Wiley-IEEE Press, 1997.
- [19] Perrott, M.H., "CppSim System Simulator Package," <http://www.cppsim.com>
- [20] R. Navid, T. H. Lee and R. W. Dutton, "Minimum achievable phase noise of RC oscillators," *IEEE J. of Solid-State Circuits*, vol. 40, no. 3, pp. 630-637, March 2005.
- [21] R. Schreier and G. C. Temes, *Understanding Delta-Sigma Data Converters*, New York: Wiley-IEEE Press, 2004.
- [22] C.P.L. van Vroonhoven, and K.A.A. Makinwa, "Linearization of a thermal-diffusivity-based temperature sensor," *IEEE Sensors*, pp. 1697-1700, Oct. 2009.
- [23] M. Park and M. Perrott, "A 0.13 $\mu$ m CMOS 78dB SNDR 87mW 20MHz BW CT  $\Delta\Sigma$  ADC with VCO-based integrator and quantizer," *Dig. Tech. ISSCC*, pp. 170-171, Feb. 2009.
- [24] K. Reddy, "A 16mW 78dB-SNDR 10MHz-BW CT- $\Delta\Sigma$  ADC using residue-cancelling VCO-based quantizer," *Dig. Tech. ISSCC*, pp. 152-154, Feb. 2012.
- [25] A. Ghosh and S. Pamarti, "Linearization Through Dithering: A 50 MHz Bandwidth, 10-b ENOB, 8.2 mW VCO-Based ADC," *IEEE J. of Solid State Circuits*, vol. 50, no. 9, pp. 2012-2024, June 2015.
- [26] IEEE Standard Definitions of Physical Quantities for Fundamental Frequency and Time Metrology---Random Instabilities," in *IEEE Std Std 1139-2008* pp.c1-35, Feb. 2009



**Uğur Sönmez** (S'10-M'15) was born in Istanbul, Turkey on 3 April 1986. He obtained his B.Sc. and M.Sc. degrees in electronics from Middle East Technical University, Ankara, Turkey in 2008 and 2011, respectively. In August 2011, he joined the Electronic Instrumentation Laboratory in TU Delft, where he is currently working towards a PhD in thermal-diffusivity-based temperature

sensors. His research interests include low-noise sensor interfaces, precision and low-power analog circuits, oversampled data converters, and time-to-digital converters.



**Fabio Sebastiano** Fabio Sebastiano (S'09-M'10) was born in Teramo, Italy in 1981. He received the B.Sc. (cum laude) and M.Sc. (cum laude) degrees in electrical engineering from University of Pisa, Italy, in 2003 and 2005, respectively. In 2006, he received the Diploma di Licenza from Scuola Superiore Sant'Anna, Pisa, Italy, and in 2011, the Ph.D. degree from Delft

University of Technology, The Netherlands.

From 2006 to 2013, he was with NXP Semiconductors Research in Eindhoven, The Netherlands, where he conducted research on fully integrated CMOS frequency references, deep-submicron temperature sensors and area-efficient interfaces for

magnetic sensors. In 2013, he joined Delft University of Technology, where he is currently an Assistant Professor. His main research interests are sensor read-outs, fully-integrated frequency references and cryogenic electronics for quantum applications. This has resulted in one book, 7 patents and over 30 technical publications.



**Kofi A. A. Makinwa** (M'97-SM'05-F'11) received the B.Sc. and M.Sc. degrees from Obafemi Awolowo University, Nigeria in 1985 and 1988 respectively. In 1989, he received the M.E.E. degree from the Philips International Institute, The Netherlands and in 2004, the Ph.D. degree from Delft University of Technology, The Netherlands.

From 1989 to 1999, he was a Research Scientist with Philips Research Laboratories, Eindhoven, The Netherlands, where he worked on interactive displays and digital recording systems. In 1999, he joined Delft University of Technology, where he is currently an Antoni van Leeuwenhoek Professor and Head of the Microelectronics Department. His main research interests are in the design of precision mixed-signal circuits, sigma-delta modulators, smart sensors and sensor interfaces. This has resulted in 10 books, 25 patents and over 200 technical papers.

Kofi Makinwa is on the program committees of the International Solid-State Circuits Conference (ISSCC), the VLSI Symposium, the European Solid-State Circuits Conference (ESSCIRC) and the Advances in Analog Circuit Design (AACD) workshop. He has also served as a guest editor of the Journal of Solid-State Circuits (JSSC) and as a distinguished lecturer of the IEEE Solid-State Circuits Society. For his doctoral research, he was awarded the 2005 Simon Stevin Gezel Award from the Dutch Technology Foundation. He is a co-recipient of several best paper awards, from the JSSC, ISSCC, Transducers and ESSCIRC among others. He is an alumnus of the Young Academy of the Royal Netherlands Academy of Arts and Sciences and an elected member of the IEEE Solid-State Circuits Society AdCom, the society's governing board.